Polymer Chemistry

ROYAL SOCIETY OF CHEMISTRY

PAPER

View Article Online
View Journal | View Issue

Cite this: *Polym. Chem.*, 2025, **16**, 3351

Cellulose nanocrystals as stabilizers for waterborne fluorescent non-isocyanate polyurethane latexes†

Hsin-Chen Chen, [a,b] Gilles Sèbe,[b] Thomas Vidil,[b] Lars A. Berglund, [c] Audrey Llevot, *[b] Qi Zhou *[a] and Henri Cramail *[b]

Received 4th April 2025,
Accepted 20th June 2025

DOI: 10.1039/d5py00341e

rsc.li/polymers

Non-isocyanate polyurethanes (NIPUs) exhibit significantly greater sustainability than conventional polyurethanes (PUs) by adhering to key principles of green chemistry, particularly the elimination of toxic chemicals. In this study, waterborne non-isocyanate polyurethane (WNIPU) latexes, exclusively stabilized by cellulose nanocrystals (CNCs) and partially derived from renewable resources, were synthesized for the first time *via* suspension polymerization. A polyaddition reaction between a siloxane diamine and 1,6-hexanediol bis(cyclic carbonate) occurred within the monomer-in-water Pickering emulsion droplets effectively stabilized with CNCs. The concentration of the CNCs was optimized for the Pickering emulsion. The CNCs acted as nanoparticle surfactants on the surface of the WNIPU latex particles, as confirmed using rhodamine B-labelled CNCs and confocal laser scanning microscopy. Spherical-shaped monomer droplets and WNIPU latex particles with a median size of 10 μm were achieved. The effect of the cyclic carbonate-to-amine molar ratio on the amine monomer conversion, molecular weight, and thermal properties of the WNIPU was investigated. The obtained WNIPU suspensions exhibited fluorescence under UV irradiation at 365 nm owing to the clustering of carbamates. Combining the fluorescence properties with low glass transition temperatures, these latexes open various potential applications as functional coatings.

1. Introduction

Polyurethanes (PUs) are ubiquitous in everyday life, being widely used in foams, coatings, elastomers, adhesives, and biomedical products. With an annual production volume of 20 kilotons and a global market value estimated at $78.07 billion in 2023, PUs hold a prominent position in the polymer industry.[1,2] However, the isocyanates used as key raw materials in most commercial PUs are associated with sustainability concerns and are recognized as toxic and harmful substances. In response to increasing regulatory restrictions on isocyanate usage and the transition to more sustainable PU alternatives, non-isocyanate polyurethanes (NIPUs) have emerged as a promising solution. Waterborne NIPUs (WNIPUs) have attracted increasing attention for their benefits in eliminating volatile organic compounds, making them particularly suitable for adhesive and coating applications. One common method for producing WNIPUs is the acetone process, which is widely used in industry for manufacturing conventional isocyanate-based waterborne polyurethanes (WPUs).[3,4] This process involves incorporating an internal emulsifier into the polymer backbone to form prepolymers in acetone, followed by neutralization using dispersing agents such as carboxylic acids or tertiary amines. The WNIPU dispersions are finally obtained after acetone removal.[5] However, this approach has limitations, including the incorporation of hydrophilic moieties that reduce water resistance and the significant acetone usage required during the process.

Mini-emulsion polymerization offers a promising alternative for hydrophobic monomers such as vegetable oils and terpenes and has been adapted for conventional WPUs.[6–8] In this method, the hydrophobic liquid monomer phase is emulsified in water containing surfactants and co-stabilizers using high-shear devices, creating small monomer droplets with increased interfacial area. These droplets are stabilized by a surfactant monolayer adsorbed on their surface, preventing coalescence due to Brownian motion, creaming or sedimentation. Additionally, highly water-insoluble co-stabilizers inhibit

[a]*Division of Glycoscience, Department of Chemistry, School of Engineering Sciences in Chemistry, Biotechnology and Health, KTH Royal Institute of Technology, AlbaNova University Centre, SE-106 91 Stockholm, Sweden. E-mail: qi@kth.se*
[b]*Univ. Bordeaux, CNRS, Bordeaux INP, LCPO, UMR 5629, F-33600 Pessac, France. E-mail: henri.cramail@enscbp.fr, audrey.llevot@enscbp.fr*
[c]*Department of Fibre and Polymer Technology, KTH Royal Institute of Technology, Teknikringen 56, SE-100 44 Stockholm, Sweden*

† Electronic supplementary information (ESI) available. See DOI: https://doi.org/10.1039/d5py00341e

Ostwald ripening by restricting monomer diffusion from smaller to larger droplets.[9] Using this approach, Cramail and colleagues successfully developed WNIPU dispersions from cyclic carbonate and diamine monomers with 30 wt% solid content and a weight-average molecular weight ($\overline{M_w}$) of 6.8–7.1 kg mol^{-1}, using surfactants Tween 80 and sodium dodecyl sulfate (SDS).[10] However, the residual surfactants in such WPU latexes have been reported to negatively affect their optical, mechanical, and adhesive properties. To address this, small-molecule surfactants have been replaced with alternatives such as macromonomers, amphiphilic copolymers, synthetic or bio-based reactive hydrophilic polymers, and solid particle stabilizers.[11–16] Among these, solid particle-stabilized emulsions, known as Pickering emulsions, require lower amounts of stabilizers and exhibit superior efficiency and stability.[16,17]

Nanocelluloses derived from renewable resources have recently received considerable attention as stabilizers for Pickering emulsions,[18–21] offering improved sustainability compared to inorganic nanoparticle stabilizers such as silica, nanoclay, metal oxides, and graphene oxide.[22–25] Cellulose nanocrystals (CNCs), produced *via* sulfuric acid hydrolysis of natural cellulose materials such as wood pulp, are rod-like particles featuring nanoscale dimensions with a length of 100–200 nm and a width of 3–20 nm, high crystallinity, surface sulfate groups carrying negative charges (0.6–1.1% sulfur by mass), and high colloidal stability in water. In addition, CNCs also possess remarkable attributes such as a high specific Young's modulus, a large specific surface area, low density, non-toxicity, biodegradability, and inherent amphiphilicity. These characteristics make CNCs highly versatile for applications as reinforcing fillers, rheology modifiers, and interfacial stabilizers in advanced composite materials.[26] CNCs have been extensively studied and demonstrated to effectively stabilize Pickering emulsions with a variety of oil phases, including alkane hydrocarbons, corn oil, coconut oil, oleic acid, and sunflower oil.[27–33] The amphiphilic nature of CNCs, arising from the surface hydroxyl groups and the hydrophobic plane (200) of their crystalline structure, enables their partitioning at the oil–water interface, as confirmed by interfacial tension measurements.[27,28] This results in the formation of discrete CNC shells at the interface, enhancing emulsion stability. To stabilize waterborne polymer latexes such as polystyrene and poly(methyl methacrylate), further surface hydrophobic functionalization of CNCs or combination with surfactants is often required.[34–39] Nonetheless, pristine CNCs that are able to stabilize hexadecane Pickering emulsions have also been applied as stabilizers for styrene, acrylates, and methacrylates to form monomer-in-water Pickering emulsions, followed by polymerization in water to produce latexes.[16,18]

To further enhance the sustainability of NIPUs, herein, we report a greener approach for synthesizing WNIPUs stabilized by the pristine CNCs. To the best of our knowledge, this is the first study to utilize pristine CNCs as a stabilizer for polyaddition polymerization in water without the use of a cosolvent, surfactant, or catalyst. Given the scarcity of relevant examples and the significant viscosity differences between NIPU monomers and common organic phases in waterborne emulsions, the primary challenge was the selection of cyclic carbonate and amine monomers with appropriate viscosities and hydrophobicities. A stable emulsion was obtained using a combination of 1,6-hexanediol bis(cyclic carbonate) (HCC) and 1,3-bis(3-aminopropyl)tetramethyldisiloxane (siloxane amine), which were selected as the monomers for this study. The effects of varying the amount of CNCs on the morphology, particle sizes, and size distribution of monomer droplets and WNIPU latexes were investigated to optimize the process and elucidate the stabilization mechanism. Monomer conversion and polymer molecular weight were monitored to identify optimal polymerization conditions. Additionally, the thermal and luminescence properties of the materials prepared from the WNIPU latexes were also investigated.

2. Experimental section

2.1. Materials

Wood CNCs in the form of a 12 wt% aqueous suspension were obtained from the University of Maine (Orono, ME, USA). The CNC sample was diluted to 1 wt% and dialyzed against ultrapure water before use. 1,6-Hexanediol diglycidyl ether was purchased from Biosynth (Staad, Switzerland). 1,3-Bis(3-aminopropyl)tetramethyldisiloxane (siloxane amine, density: 0.897 g mL^{-1}) was purchased from abcr GmbH (Karlsruhe, Germany) and used as received. Sodium chloride (NaCl), tetrabutylammonium iodide (TBAI), and rhodamine B isothiocyanate (RBITC) were purchased from Merck KGaA (Darmstadt, Germany) and used as received.

2.2. Preparation of fluorescent-labeled CNCs

Fluorescent labeling of CNCs was achieved *via* the formation of thiocarbamate linkages between the hydroxy groups on the CNCs and the isothiocyanate groups of RBITC.[40] 20 mg of RBITC was added to 100 mL of a 1 wt% CNC water suspension containing 0.1 M NaOH. The reaction proceeded at room temperature in the dark for 72 hours with stirring. The RBITC-labeled CNCs (CNC-RB) were separated by centrifugation, washed with 0.1 M NaOH and dialyzed against ultrapure water for 5 days. The purified CNC-RB was maintained in 1 wt% water suspension in a 4 °C refrigerator.

2.3. Synthesis of 1,6-hexanediol bis(cyclic carbonate)

1,6-Hexanediol diglycidyl ether was mixed with 2.5 mol% of TBAI and transferred into a Büchiglasuster laboratory pressure reactor (Uster, Switzerland) for carbonation. The reactor was sealed with gas inlets and outlets and then stirred at 500 rpm using a magnetically coupled stirrer. CO_2 was introduced at room temperature for 5 minutes, followed by heating the reactor to 80 °C while maintaining continuous CO_2 bubbling for 24 hours. The conversion of oxirane moieties to cyclic carbonates was confirmed using ^{1}H NMR (Fig. S1, ESI†). The resulting 1,6-hexanediol bis(cyclic carbonate) (HCC) with a

measured density of 1.224 g cm^{-3} was obtained as a transparent liquid with complete conversion (>99%).

2.4. Preparation of monomer droplets and WNIPU latexes

The organic phase was prepared by mixing HCC and siloxane amine at room temperature, with the monomer mixture fixed at 10 wt% of the total emulsion. The aqueous phase was prepared by dispersing CNCs in ultrapure water under tip-sonication (Branson SFX550 Sonifier), in which 75 mM NaCl was added to partially screen the charges on the CNCs. The organic phase was then added dropwise to the aqueous phase and emulsified using a laboratory disperser (IKA T 25 digital Ultra-Turrax) at 15 000 rpm for 15 seconds, forming monomer-in-water droplets. Polymerization was subsequently conducted at 60 °C for 24 hours under mechanical stirring at 200 rpm, and the resulting latexes were cooled to room temperature.

2.5. Characterization

The rod-like morphology of the wood-derived CNCs was characterized by atomic force microscopy (AFM). The AFM height image and the corresponding histograms of width and length distributions are presented in Fig. S2, ESI.† The CNCs exhibited an average width of 5.9 ± 1.5 nm and an average length of 201.9 ± 70.7 nm. A dilute water suspension of CNCs was deposited on a plasma-treated silicon wafer and air-dried at room temperature, and the image was recorded in ScanAsyst mode using a silicon cantilever with a force constant of 0.4 N m^{-1} and a resonance frequency of 70 kHz. The viscosities of the monomers in mPa s were measured by a frequency sweep test from 0.01 to 1000 s^{-1} using a 25 mm cone plate with a 2° cone angle (CP25-2°) on a modular compact rheometer MCR 302 (Anton Paar). The morphology of the droplets and latexes was examined through confocal laser scanning microscopy (Zeiss LSM 800, Carl Zeiss AG, Oberkochen, Germany) equipped with an Airyscan detection unit. ZEN Blue 2.1 software was used to process the acquired datasets. Droplet and latex sizes and size distributions were determined using a MasterSizer 3000 (Malvern), with samples dispersed in the manual dispersion chamber filled with deionized water. The fluorescence properties of the WNIPU latexes were analyzed using a ClarioStar plate reader (BMG Labtech). ^{1}H NMR spectra were acquired using a Bruker Avance 400 MHz spectrometer using a mixture of $CDCl_3$ and DMSO-d_6 (1 : 1, v/v) as the deuterated solvent. The molecular weights of the WNIPUs were measured by size exclusion chromatography (SEC) in chloroform with triethylamine at 30 °C (flow rate: 0.8 mL min^{-1}) using Agilent PLgel columns (PLgel 5 μm Guard, 7.5 mm × 50 mm, and PLgel Mixed C, 7.5 mm × 300 mm). Differential Scanning Calorimetry (DSC) was performed on a Mettler Toledo DSC instrument at a heating rate of 10 °C min^{-1} under nitrogen flow (50 mL min^{-1}). The thermal program consisted of two heating cycles from −80 °C to 150 °C, with a cooling cycle in between. The glass transition temperature (T_g) of the samples was determined from the second heating cycle.

3. Results and discussion

3.1. Pickering emulsification of the NIPU monomers in water

The selection of siloxane diamine and 1,6-hexanediol bis (cyclic carbonate) as the monomer pair was guided by several key criteria. First, to facilitate successful suspension polymerization within the droplets, the monomers needed to exhibit sufficient hydrophobicity. Second, low viscosity was desirable to support the emulsification process and enable the formation of spherical droplets, which are essential for evaluating and understanding the stabilization mechanism. Finally, miscibility between the selected diamine and the cyclic carbonate was crucial to ensure homogeneous polymerization. To optimize the CNC concentration for stable monomer-in-water emulsions, the mass of CNC particles (m_p) was varied from 1 to 10 mg per mL of NIPU monomers. The organic phase consisted of HCC and siloxane amine monomers at a fixed molar ratio of 1 : 1. The monomer-to-water ratio was maintained at 10 : 90 by weight for all tested emulsions. The organic phase was added dropwise to the aqueous phase containing the desired amount of well-dispersed CNC particles and emulsified through high-shear mixing using an Ultra-Turrax disperser, resulting in the formation of monomer-in-water droplets, as shown in Fig. 1a.

After storage at 22 °C for 3 h, sedimentation of the emulsions was observed due to the high density of the monomer mixture (1.06 g cm^{-3}), calculated based on the densities of HCC and siloxane amine. The emulsion volume gradually increased with increasing m_p of the CNC (Fig. 1b). When m_p was lower than 3 mg mL^{-1}, the organic phase separated from the aqueous phase and adhered to the surface of the plastic tube. In contrast, when m_p exceeded 3 mg mL^{-1}, the sedimen-

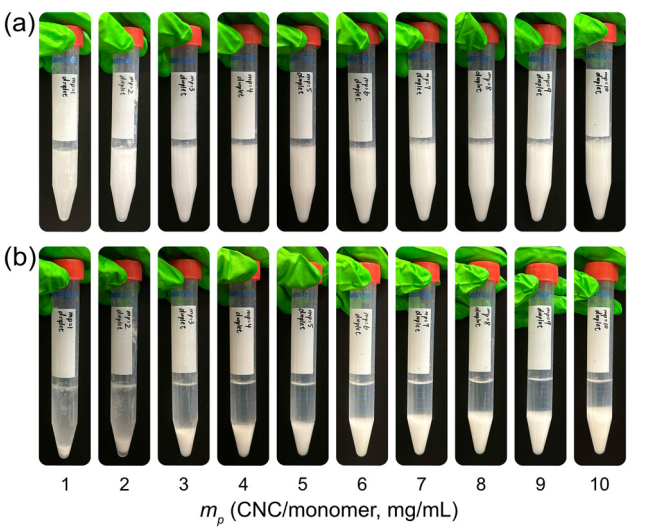

Fig. 1 HCC/siloxane amine/aqueous CNC emulsion stability with increasing CNC concentration in the aqueous phase. Photographs of (a) the emulsions freshly prepared using Ultra-Turrax, and (b) the emulsions stored for 3 h after emulsification.

ted emulsion could be easily redispersed in water by brief shaking using a vortex mixer.

The size distribution of HCC/siloxane amine droplets in emulsions stabilized with varying concentrations was analyzed using a Mastersizer (Fig. 2a). All emulsions were characterized 3 h after emulsification to ensure stabilization *via* the limited coalescence process.[18] Prior to measurement, the samples were redispersed using a vortex mixer. At $m_p \geq 4$ mg mL^{-1}, a single, narrow size distribution was observed, indicating the formation of uniform droplets. In contrast, at $m_p = 3$ mg mL^{-1}, an additional peak appeared at a larger size, suggesting the presence of a secondary droplet population, likely due to incomplete stabilization and coalescence. These results demonstrate that increasing CNC concentration enhances droplet uniformity and prevents phase separation. A smaller size component within the range of 350–1000 nm, with a peak around 600 nm, was also observed in all size distribution plots. As the CNCs exhibit a length distribution ranging from 50 to 300 nm (Fig. S2†), this submicron-sized component likely corresponds to a smaller population of monomer droplets stabilized by small CNC nanoparticles that remained as discrete entities rather than coalescing into larger, micron-sized droplets.

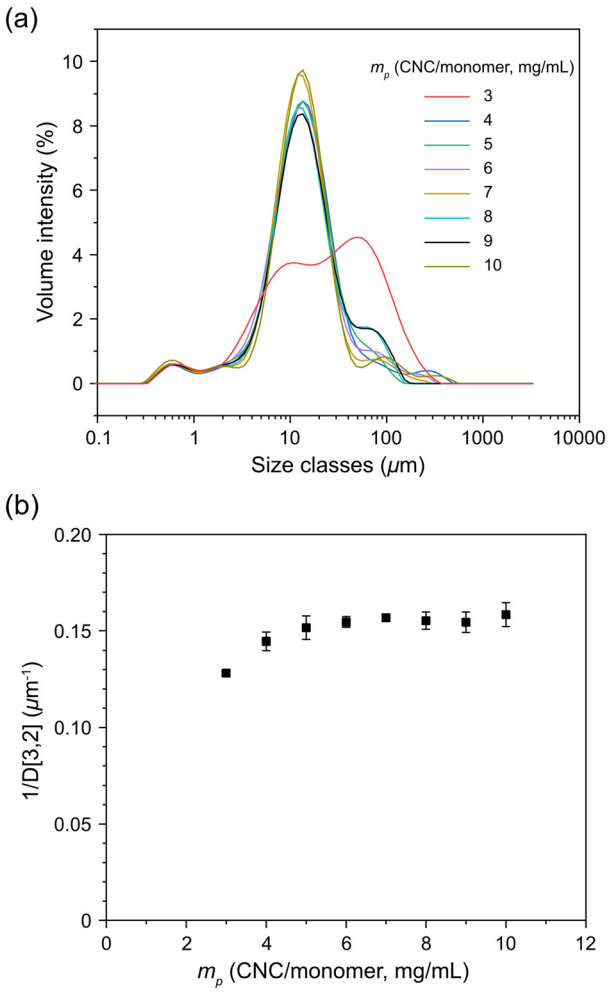

Fig. 2 (a) Size distribution and (b) the inverse $D[3,2]$ average diameters of the HCC/siloxane amine emulsion droplets as a function of CNC concentration (m_p of 3 to 10 mg mL^{-1}).

The Sauter diameters ($D[3,2]$) of the HCC/siloxane amine emulsion droplets were calculated from their size distributions. The average reciprocal diameter ($1/D[3,2]$) was plotted as a function of CNC concentration (m_p) in Fig. 2b. A linear increase in $1/D[3,2]$ was observed as the CNC concentration increased between 3 and 5 mg mL^{-1}, consistent with the limited coalescence mechanism, which is characteristic of successful Pickering emulsion formation. In the nanoparticle-deficient region (low m_p), droplets generated by shear-induced emulsification initially coalesce to reduce the interfacial area until a sufficient number of CNC nanoparticles adsorb onto their surfaces, stabilizing them. At CNC concentrations exceeding 5 mg mL^{-1}, the droplets were rapidly stabilized upon agitation, preventing further coalescence, as the available CNC nanoparticles surpassed the amount required to cover the generated interfacial area. The average $D[3,2]$ of the droplets reached a plateau at 6.5 ± 0.2 μm, indicating that the particle-rich region began at a CNC concentration of 6 mg mL^{-1}.[8,41] Interestingly, even though the droplet size had reached a constant plateau, the emulsion volume was observed to gradually increase with increasing CNC content (Fig. 1b). This phenomenon is attributed to the increased viscosity of the continuous aqueous phase resulting from the higher CNC concentration, which in turn retards the sedimentation of the monomer droplets.[42,43] The surface coverage (C) of CNCs on the monomer droplets can be estimated based on the following equation:[18]

$$C = \frac{m_p D}{6h\rho V_{oil}}$$

where D is the $D[3,2]$ average radius of the droplets, h is the average width (thickness) of the CNCs (5.9 nm as measured by AFM), ρ is the CNC density (1.5 g cm^{-3}), and V_{oil} is the volume of the monomers. The surface coverage of CNCs was calculated to be 96.5% at $m_p = 8$ mg mL^{-1}.

3.2. Suspension polymerization of the NIPU monomer emulsions

WNIPU latexes were synthesized *via* suspension polymerization, where a polyaddition reaction between the diamine and bis(cyclic carbonate) occurred within the HCC/siloxane amine emulsion droplets dispersed in water. Advantageously, this process does not require the use of a catalyst or surfactant, which is uncommon in waterborne latex production. While the stability of dispersed phases in waterborne systems is typically maintained by the surfactants before, during and after polymerization,[44,45] in this study, latex stability was ensured exclusively by the CNCs. The polymerization conditions, previously established at 60 °C for 24 h,[10] were applied without further optimization. To maintain the monomer droplet dispersion in water and prevent clustering or destabilization during heating, stirring at 200 rpm was performed during

polymerization. The size distribution of latex was determined and compared to that of the dispersed monomer droplets prior to polymerization (Fig. 3a). The formulation with a CNC concentration (m_p) of 4 mg mL^{-1} exhibited two major peaks in the latex size distribution. It has to be noted that although uniform droplets formed at a CNC m_p of 4 mg mL^{-1} in the monomer emulsion, this concentration was insufficient to ensure dispersion stability during polymerization. Adequate interfacial coverage by CNC nanoparticles is required to prevent the uncovered surfaces of the monomer droplets from interacting, which could lead to size variations or potential destabilization during polymerization. A CNC m_p of 6 mg mL^{-1} was the minimum requirement for stable latex polymerization, producing monodisperse latexes. However, the size distribution was broader and shifted toward smaller sizes compared to that of the monomer emulsion droplets. At a CNC m_p of 8 mg mL^{-1}, monodisperse latexes with a size distribution similar to that of the monomer droplets were achieved. The median particle size (Dx(50)) of the droplets and latexes were 12.7 ± 0.3 μm and 9.7 ± 0.1 μm, respectively, demonstrating that the polyaddition occurred within the initially formed droplets and that the selected monomers were sufficiently hydrophobic to sustain stable suspension polymerization in an aqueous medium.

NIPUs have been reported to exhibit fluorescence properties due to the aggregation of carbamates, leading to clusterization-triggered emission (CTE).[46–48] This phenomenon, previously observed in conventional PUs,[49] lowers the band gap for the transition from the ground state to the excited state.[50] In this study, we exploited this property to characterize the latexes using confocal laser scanning microscopy (Fig. 3b). Interestingly, upon excitation with a 405 nm laser, the WNIPU

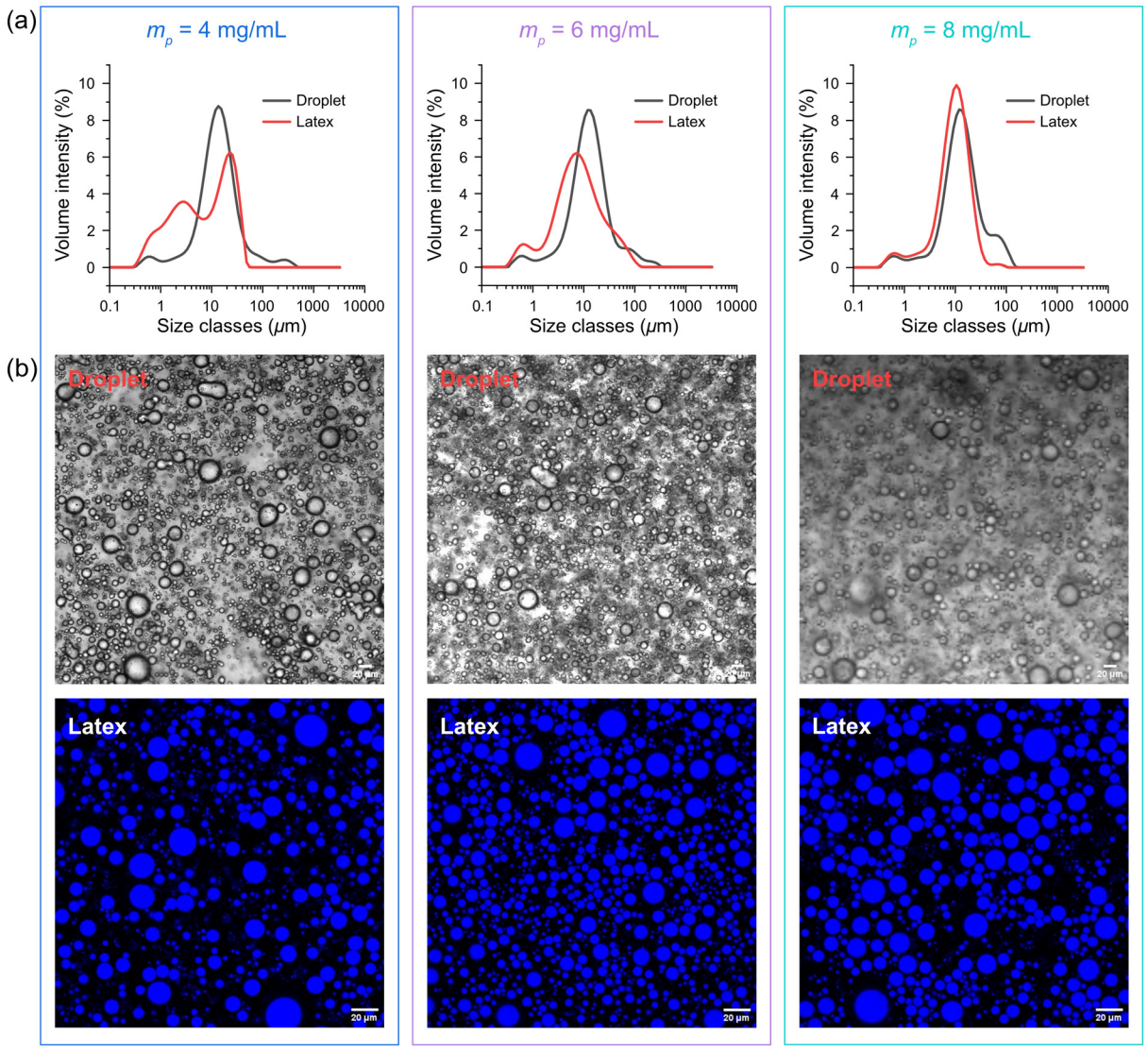

Fig. 3 (a) Size distributions and (b) confocal microscopy images of the HCC/siloxane amine emulsion droplets and WNIPU latexes with CNC concentrations (m_p) of 4, 6, and 8 mg mL^{-1}. Scale bar: 20 μm.

latexes exhibited fluorescence, whereas the monomer droplets did not, indicating successful suspension polymerization. Both droplets and latexes featured a spherical shape, which is attributed to the combined effects of the appropriate viscosity of the dispersed monomer phase and the optimized shearing speed for emulsification of the monomer droplets using Ultra-Turrax. Indeed, the low viscosity of the monomer mixture (2700 mPa s at a shear rate of 0.1 s^{-1}) allowed them to undergo shape relaxation during the shearing process, facilitating the formation of uniform spherical droplets. This is in contrast with the irregularly shaped emulsions observed in previous studies, where a high-viscosity organic dispersed phase was used.[8] Furthermore, the droplet and latex size distributions obtained from confocal laser scanning microscopy, analyzed *via* image analysis, are presented in Fig. S3, ESI.† The results are consistent with those obtained from the MasterSizer, confirming that a CNC concentration of 8 mg mL^{-1} produces similar droplet and latex sizes before and after polymerization. The average droplet diameter was 12.6 ± 3.7 μm, while the average latex particle diameter was 10.2 ± 3.1 μm, supporting the conclusion that the polymerization occurred within the initially formed spherical droplets.

The role of CNCs as stabilizers in WNIPU latexes was visualized using CNCs labeled with rhodamine B (CNC-RB). As CNC-RB exhibits an absorption maximum in the 550–570 nm range,[40] both blue and red fluorescence from WNIPU and CNC-RB were observed upon excitation with 405 nm and 561 nm lasers, respectively (Fig. 4). A red contour surrounding the blue WNIPU spheres indicated that the CNC-RB was localized at the interface, confirming its role as a stabilizer. The nearly complete coverage of CNCs on the latex particle surface corroborates the calculated surface coverage of 96.5% at an m_p of 8 mg mL^{-1}. These findings demonstrate the successful formation of the CNC-WNIPU Pickering latex.

The structure of the WNIPU latex obtained using the optimal CNC concentration (m_p of 8 mg mL^{-1}) and an HCC/amine ratio of 1.0 was characterized by ^1H NMR in a 1 : 1 (v/v) mixture of $CDCl_3$ and DMSO-d_6 and SEC.[51] Compared to the starting cyclic carbonate and amine, the appearance of the proton peaks b′ at δ = 4.68 ppm, a″ at 3.80–3.98 ppm, b″ at 3.75 ppm, c′ at 3.58 ppm, a′ at 3.45 ppm, c″ at 3.27 ppm, and g′ at 2.93 ppm confirmed the aminolysis of the cyclic carbonate and the formation of polyhydroxyurethane (Fig. 5). Additionally, no residual peaks a and b, characteristic of the cyclic carbonate, were observed, indicating a complete conversion of cyclic carbonate. A residual amine peak g at 2.58 ppm, corresponding to the proton at the α-position of the amine group, was detected. The amine conversion, calculated from the integration of peak g and peak g′, reached 73.2%. The molecular weight and dispersity of the synthesized WNIPU were determined by SEC using chloroform as the eluent (Fig. S5 ESI†). A number-average molecular weight ($\overline{M_n}$) of 2700 g mol^{-1}, a weight-average molecular weight ($\overline{M_w}$) of 5500 g mol^{-1}, and a dispersity ($Đ$) of 2.0 were determined.

Unlike conventional PUs, which are synthesized through the reaction of isocyanates with hydroxy groups, NIPUs follow a different reaction pathway. Polymerization within the droplets proceeded *via* a polyaddition reaction between bis(cyclic carbonate)s and diamines. Therefore, no covalent chemical interaction between the CNCs and the polymer matrix was expected. This was supported by NMR analysis, which showed no evidence of CNC involvement in the polymerization under the employed conditions at 60 °C for 24 h.

3.3. Effect of the HCC/siloxane amine ratio

To further optimize the conversion of siloxane amine in this suspension polymerization, the HCC/amine molar ratio was further varied from the initial 1.0 to 0.9, 1.1, and 1.2, while the CNC concentration was fixed at the optimal m_p of 8 mg mL^{-1}. The droplet size distributions at various HCC/amine ratios (Fig. 6a) showed a unimodal profile for ratios of 0.9 and 1.0, while shoulder peaks and broader size distributions were observed at higher ratios of 1.1 and 1.2. This phenomenon was primarily attributed to differences in viscosity between the two monomers: HCC exhibits significantly higher viscosity (1400 mPa s at a shear rate of 0.1 s^{-1}) compared to the siloxane amine (200 mPa s). As a result, increasing the HCC content

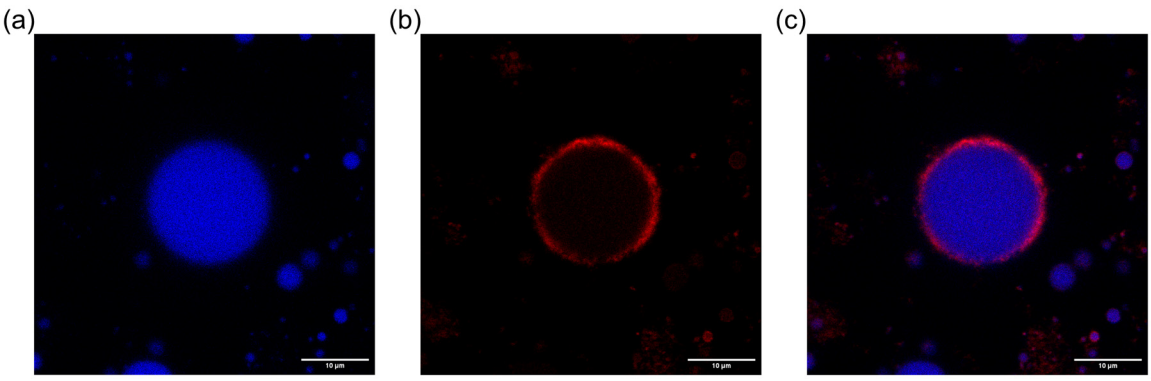

Fig. 4 Confocal laser scanning microscopy (CLSM) images of the WNIPU latex stabilized with CNC-RB at an m_p of 8 mg mL^{-1}. (a) Fluorescence detected under 405 nm excitation (WNIPU), (b) fluorescence detected under 561 nm excitation (CNC-RB), and (c) merged image of both channels. Scale bar: 10 μm.

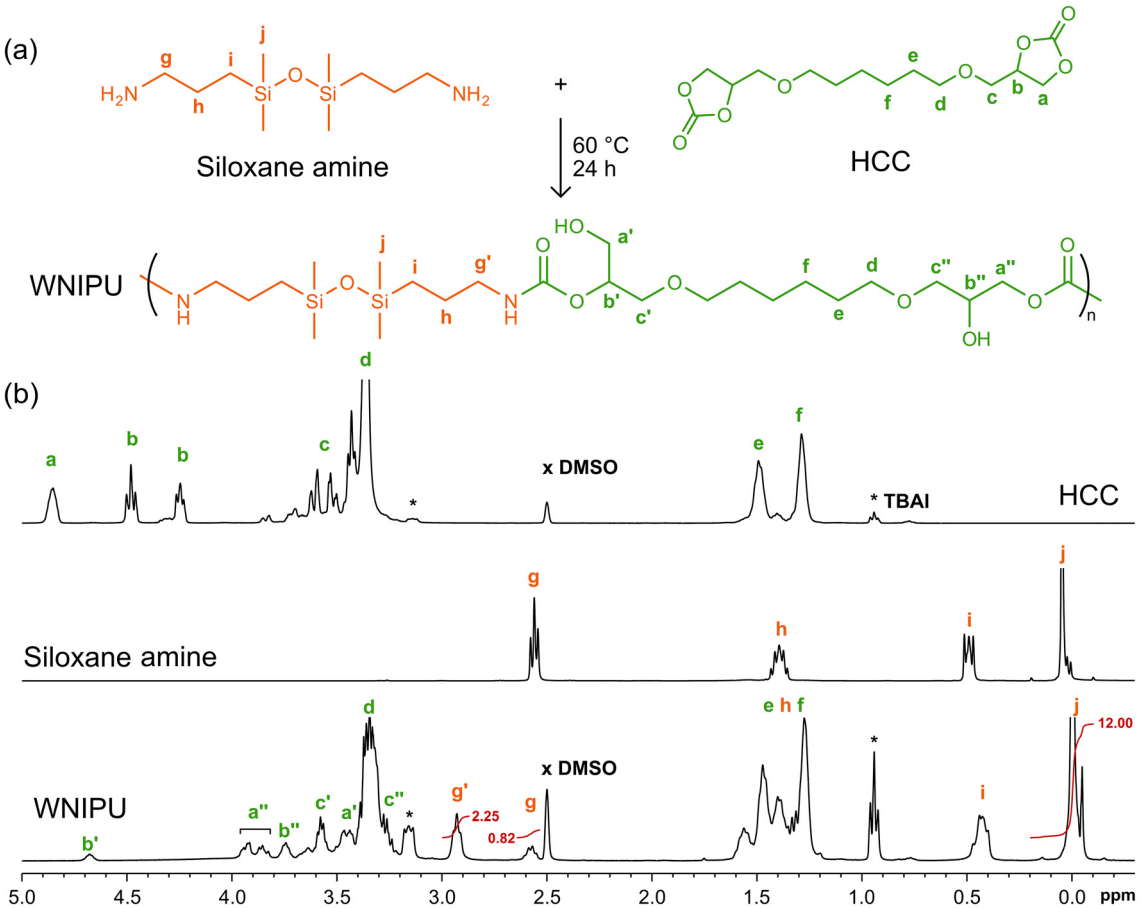

Fig. 5 (a) Reaction scheme between siloxane amine and HCC. (b) ^{1}H NMR spectra of starting monomers HCC, siloxane amine and the dried WNIPU latex with an HCC/amine ratio of 1.0 in a mixture of $CDCl_3$ and DMSO-d_6.

raised the viscosity of the organic phase, hindering the formation of uniformly sized droplets during emulsification. In addition, the composition of the oil phase also influenced the emulsification efficiency of CNCs. Previous studies have shown that the wettability of CNCs with respect to the organic phase significantly affects the resulting droplet.[33,52] Variations in the polarity and hydrophobicity of the oil phase can alter the interfacial affinity of CNCs, thereby impacting their ability to stabilize droplets and leading to differences in droplet size distributions.[53] After suspension polymerization, monodisperse WNIPU latexes with a narrow size distribution were obtained at HCC/amine ratios of 0.9 and 1.0 (Fig. 6b). Further increasing the HCC content resulted in the formation of two predominant size population peaks in the WNIPU latex. For the investigated HCC/amine ratios, no trace of unreacted cyclic carbonates was detected (Fig. S4, ESI†). Increasing the HCC/amine ratio led to a slight increase in the conversion of siloxane amine. The highest amine group conversion of 86.3% was achieved at an HCC/amine ratio of 1.1, corresponding to a 13% increase compared to a ratio of 1.0 (Fig. 6c). Consequently, the resulting WNIPU polymer exhibited the highest $\overline{M_w}$ of 5700 g mol^{-1} and an $\overline{M_n}$ of 2800 g mol^{-1}, as determined by SEC analysis (Fig. S5, ESI†).

Bourguignon *et al.*[54] reported hydrolysis of cyclic carbonate in the WNIPU hydrogels, evidenced by a gradual pH decrease due to H_2CO_3 formation. To limit the hydrolysis of five-membered cyclic carbonates, pH was adjusted in the 10.5–11.5 range to prepare NIPU hydrogels using water soluble bis(cyclic carbonates) and polyamine. Indeed, we also observed a gradual decrease in pH from 9.8 to 8.4 for the HCC/siloxane amine emulsion (HCC : amine = 1.1 : 1) in water during the 4-hour suspension polymerization. Thus, a portion of the HCC may undergo hydrolysis upon contact with water during the polymerization rather than participating in the reaction with the siloxane amine. Therefore, the pH of the water suspension was maintained at 10 using a 50 mM ammonium hydroxide buffer throughout the polymerization. However, the resulting amine conversion was 86.8%, which was not significantly affected as compared to that (86.3%) without buffer (Fig. S6, ESI†). On the other hand, when the HCC/amine ratio was 1.0, the amine conversion increased from 73.2% to 82.6% after introducing the buffer to maintain the pH at 10 in the polymerization reaction (Fig. S7, ESI†). These results suggest that while pH control is critical to the polyaddition reaction, optimizing the HCC/amine ratio plays a more significant role in maximizing amine conversion to WNIPU.

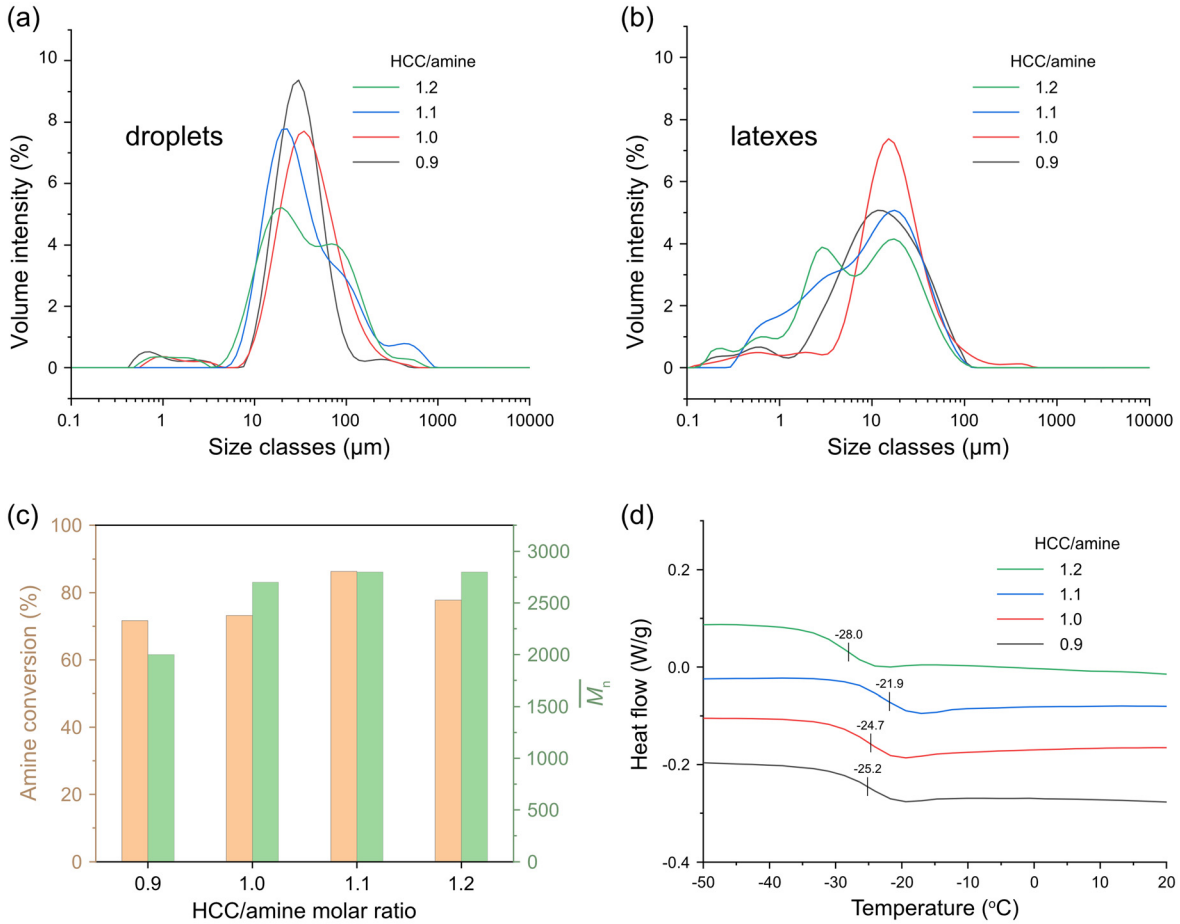

Fig. 6 Effect of the HCC/amine ratio on (a) droplet size distribution, (b) latex size distribution, and (c) amine conversion determined by ^{1}H NMR and $\overline{M}_n$ determined using polystyrene standards on SEC, and (d) DSC thermograms from the second heating ramp of WNIPU latexes stabilized with a CNC concentration at an m_p of 8 mg mL^{-1}.

The thermal properties of the WNIPUs were analyzed by DSC (Fig. 6d). All polymers were amorphous, with glass transition temperatures (T_g) ranging from −30 °C to −20 °C. Due to the relatively lower molecular weight of these WNIPUs compared to conventional polymers, their T_g temperatures were affected by their molecular weight. The WNIPU synthesized at an HCC/amine ratio of 1.1 exhibited the highest T_g of −21.9 °C, which correlates well with its highest molecular weight in the series. The low T_g values of these aliphatic linear WNIPUs impart flexibility and tackiness, making them promising candidates for applications in coatings.

3.4. Fluorescence behavior of the WNIPU latex

The fluorescence properties of aqueous WNIPU latex suspensions were characterized. A 10 wt% WNIPU latex suspension was synthesized from an aqueous monomer emulsion (HCC/amine molar ratio of 1.1) stabilized by CNCs, with an m_p of 8 mg mL^{-1}, through suspension polymerization. The obtained 10 wt% aqueous WNIPU latex suspension was diluted to 7.5, 5, 2.5, and 1 wt% (Fig. 7a). Interestingly, even at a dilution of 1 wt%, the latex suspension showed weak but visible emission (Fig. 7b). This behavior is different from that of DMF solutions of fluorescent PU, where dilute solutions were non-luminescent due to the absence of intermolecular interactions among PU molecules, particularly the –NHCOO– units, as explained by the clustering-triggered emission (CTE) mechanism of non-conventional luminogens.[49] In contrast, because the WNIPU molecules were confined within the latex particles, dilution in water did not eliminate their luminescence properties, apart from a reduction in emission intensity. The fluorescence spectra of the aqueous latex suspensions showed a maximum emission wavelength at 443 nm and maximum excitation wavelengths at 364 and 377 nm (Fig. 7c), consistent with previously reported aliphatic polyhydroxyurethane with fluorescence attributed to the clustering of carbamates.[47,48] Furthermore, the aqueous WNIPU latex suspension was used as ink to write the letters “NIPU” on a glass slide. Upon drying, the letters formed a coating approximately 100 μm thick and exhibited a bright light blue fluorescence under UV irradiation at 365 nm (Fig. 7d). The glowing fluorescence was even observed through the edges of the glass slide.

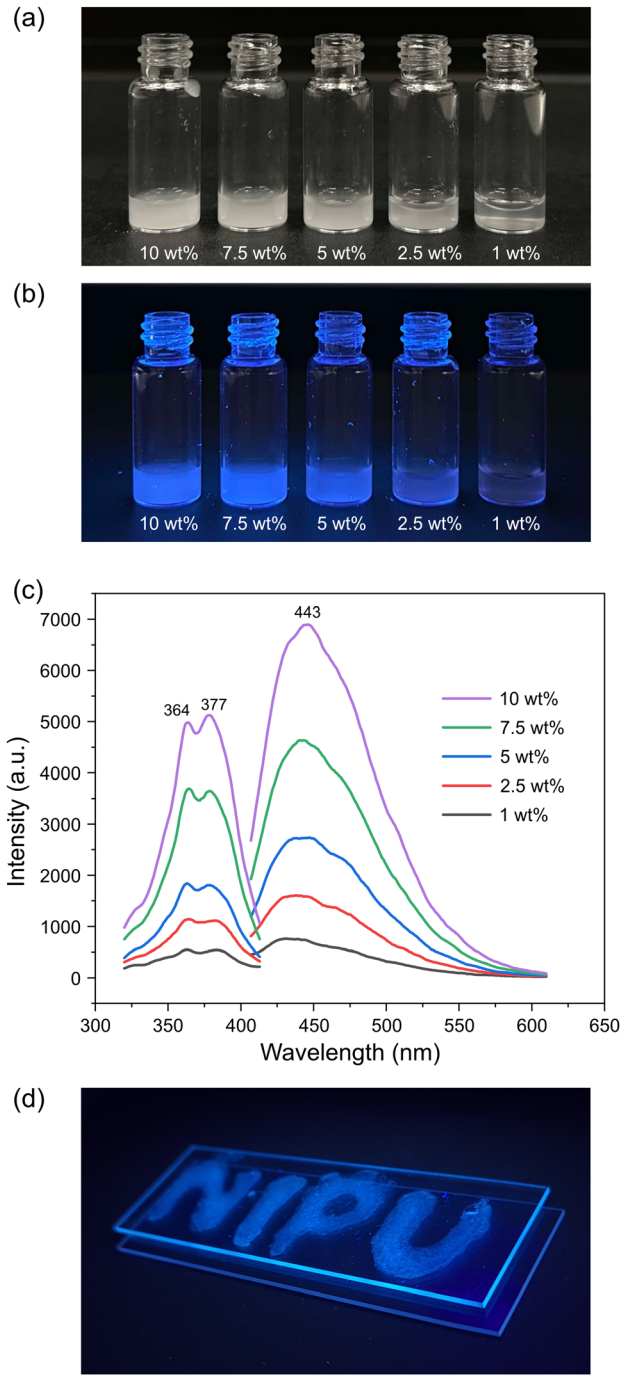

Fig. 7 Photographs and fluorescence spectra of the aqueous WNIPU latex suspensions with varying solid contents. (a) Photographs taken under nature light, (b) photographs taken under UV irradiation (λ = 365 nm), and (c) excitation and emission spectra recorded with aqueous suspensions. (d) Photograph of the letters "NIPU" written on a glass slide using the aqueous WNIPU latex suspension as ink, taken under 365 nm UV light (letters were written on the top glass slide).

4. Conclusion

CNC-stabilized WNIPU latexes were successfully synthesized using 1,6-hexanediol bis(cyclic carbonate) and 1,3-bis(3-aminopropyl)tetramethyldisiloxane, which exhibited suitable viscosity, hydrophobicity, and miscibility. The size of the monomer-in-water droplets was inversely correlated with the CNC concentration in the emulsions, following a trend characteristic of Pickering emulsions. When the droplet surface was sufficiently covered by CNCs at an m_p value of above 8 mg mL^{-1}, the WNIPU latexes retained particle sizes comparable to those droplets observed prior to polymerization. Optimizing the HCC/amine ratio to compensate for partial hydrolysis of cyclic carbonate in water revealed that a ratio of 1.1 achieved the highest monomer-to-polymer conversion, molecular weight, and T_g. The spherical morphology of the resulting WNIPU particles was visualized by confocal laser scanning microscopy without the need for external fluorophores, which is attributed to the CTE mechanism. This fluorescence behavior was observed in both aqueous latex suspensions and the dry NIPU. By leveraging fluorescence properties, these sustainable WNIPU materials show strong potential for functional coating applications in sensing, imaging, or anti-counterfeiting technologies.

Author contributions

Hsin-Chen Chen: conceptualization, data curation, formal analysis, investigation, visualization, and writing – original draft. Gilles Sèbe: conceptualization, supervision, and writing – review. Thomas Vidil: supervision and writing – review. Lars A. Berglund: supervision and writing – review. Audrey Llevot: conceptualization, funding acquisition, resources, supervision, and writing – review & editing. Qi Zhou: conceptualization, visualization, funding acquisition, resources, supervision, and writing – review & editing. Henri Cramail: conceptualization, funding acquisition, resources, supervision, and writing – review.

Conflicts of interest

There are no conflicts to declare.

Data availability

The data supporting this article have been included as part of the ESI.†

Acknowledgements

We thank the NIPU-EJD project for its financial support, funded by the European Union's Horizon 2020 research and innovation programme under the Marie Skłodowska-Curie grant agreement No. 955700.

References

1 R. Geyer, J. R. Jambeck and K. L. Law, *Sci. Adv.*, 2017, **3**, e1700782.
2 A. Delavarde, G. Savin, P. Derkenne, M. Boursier, R. Morales-Cerrada, B. Nottelet, J. Pinaud and S. Caillol, *Prog. Polym. Sci.*, 2024, **151**, 101805.
3 A. Gomez-Lopez, F. Elizalde, I. Calvo and H. Sardon, *Chem. Commun.*, 2021, **57**, 12254–12265.
4 J. Wu, X. Wu, C. Mu, C. Wang and W. Lin, *Prog. Org. Coat.*, 2024, **188**, 108174.
5 A. Bossion, I. Olazabal, R. H. Aguirresarobe, S. Marina, J. Martín, L. Irusta, D. Taton and H. Sardon, *Polym. Chem.*, 2019, **10**, 2723–2733.
6 B. G. Zanetti-Ramos, E. Lemos-Senna, V. Soldi, R. Borsali, E. Cloutet and H. Cramail, *Polymer*, 2006, **47**, 8080–8087.
7 H. Liu, T. Hu, D. Wang, J. Shi, J. Zhang, J.-X. Wang, Y. Pu and J.-F. Chen, *Chem. Eng. Process.*, 2019, **136**, 36–43.
8 M. Save, M. L. Hellaye, V. de Villedon, I. Adoumaz, M. Pillet, L. Atanase, M. Lahcini, E. Deniau, A. Khoukh, V. Pellerin, I. Ly, V. Dulong and V. Schmitt, *Biomacromolecules*, 2022, **23**, 2536–2551.
9 W. Ostwald, *Z. Phys. Chem.*, 1901, **37**, 385.
10 E. Rix, E. Grau, G. Chollet and H. Cramail, *Eur. Polym. J.*, 2016, **84**, 863–872.
11 H. Ahmad and K. Tauer, *Macromolecules*, 2003, **36**, 648–653.
12 M. Save, M. Manguian, C. Chassenieux and B. Charleux, *Macromolecules*, 2005, **38**, 280–289.
13 B. Charleux, G. Delaittre, J. Rieger and F. D'Agosto, *Macromolecules*, 2012, **45**, 6753–6765.
14 S. L. Canning, G. N. Smith and S. P. Armes, *Macromolecules*, 2016, **49**, 1985–2001.
15 I. Martin-Fabiani, J. Lesage, J. L. de la Haye, M. Schulz, Y. Liu, M. Lee, B. Duffy, F. D'Agosto, M. Lansalot and J. L. Keddie, *ACS Appl. Mater. Interfaces*, 2018, **10**, 11221–11232.
16 C. J. Saelices, M. Save and I. Capron, *Polym. Chem.*, 2019, **10**, 727–737.
17 I. Capron, O. J. Rojas and R. Bordes, *Curr. Opin. Colloid Interface Sci.*, 2017, **29**, 83–95.
18 I. Kalashnikova, H. Bizot, B. Cathala and I. Capron, *Langmuir*, 2011, **27**, 7471–7479.
19 I. Kalashnikova, H. Bizot, P. Bertoncini, B. Cathala and I. Capron, *Soft Matter*, 2013, **9**, 952–959.
20 M. Gestranius, P. Stenius, E. Kontturi, J. Sjöblom and T. Tammelin, *Colloids Surf., A*, 2017, **519**, 60–70.
21 C. J. Saelices and I. Capron, *Biomacromolecules*, 2018, **19**, 460–469.
22 M. J. Percy, C. Barthet, J. C. Lobb, M. A. Khan, S. F. Lascelles, M. Vamvakaki and S. P. Armes, *Langmuir*, 2000, **16**, 6913–6920.
23 X. Song, Y. Zhao, H. Wang and Q. Du, *Langmuir*, 2009, **25**, 4443–4449.
24 M. M. Gudarzi and F. Sharif, *Soft Matter*, 2011, **7**, 3432.
25 B. Brunier, N. Sheibat-Othman, M. Chniguir, Y. Chevalier and E. Bourgeat-Lami, *Langmuir*, 2016, **32**, 6046–6057.
26 Y. Habibi, L. A. Lucia and O. J. Rojas, *Chem. Rev.*, 2010, **110**, 3479–3500.
27 I. Kalashnikova, H. Bizot, B. Cathala and I. Capron, *Biomacromolecules*, 2012, **13**, 267–275.
28 Z. Hu, T. Patten, R. Pelton and E. D. Cranston, *ACS Sustainable Chem. Eng.*, 2015, **3**, 1023–1031.
29 L. Liu, Z. Hu, X. Sui, J. Guo, E. D. Cranston and Z. Mao, *Ind. Eng. Chem. Res.*, 2018, **57**, 7169–7180.
30 S. Hedjazi and S. H. Razavi, *Int. J. Biol. Macromol.*, 2018, **106**, 489–497.
31 Z. Deng, J. Jung, J. Simonsen and Y. Zhao, *Food Hydrocolloids*, 2018, **84**, 229–237.
32 A. Mackie, S. Gourcy, N. Rigby, J. Moffat, I. Capron and B. Bajka, *Nanoscale*, 2019, **11**, 2991–2998.
33 S. A. Kedzior, V. A. Gabriel, M. A. Dube and E. D. Cranston, *Adv. Mater.*, 2021, **33**, e2002404.
34 A. B. Elmabrouk, T. Wim, A. Dufresne and S. Boufi, *J. Appl. Polym. Sci.*, 2009, **114**, 2946–2955.
35 W. Du, J. Guo, H. Li and Y. Gao, *ACS Sustainable Chem. Eng.*, 2017, **5**, 7514–7523.
36 S. A. Kedzior, H. S. Marway and E. D. Cranston, *Macromolecules*, 2017, **50**, 2645–2655.
37 S. A. Kedzior, M. A. Dubé and E. D. Cranston, *ACS Sustainable Chem. Eng.*, 2017, **5**, 10509–10517.
38 A. Werner, V. Schmitt, G. Sèbe and V. Héroguez, *Polym. Chem.*, 2017, **8**, 6064–6072.
39 Y. Zhang, V. Karimkhani, B. T. Makowski, G. Samaranayake and S. J. Rowan, *Macromolecules*, 2017, **50**, 6032–6042.
40 T. Leng, Z. J. Jakubek, M. Mazloumi, A. C. W. Leung and L. J. Johnston, *Langmuir*, 2017, **33**, 8002–8011.
41 V. Maingret, V. Schmitt and V. Heroguez, *Carbohydr. Polym.*, 2021, **269**, 118261.
42 Y. Z. Aw, H. P. Lim, L. E. Low, C. K. S. Singh, E. S. Chan and B. T. Tey, *LWT–Food Sci. Technol.*, 2022, **159**, 113249.
43 W. W. Mwangi, K. W. Ho, B. T. Tey and E. S. Chan, *Food Hydrocolloids*, 2016, **60**, 543–550.
44 B. Bizet, E. Grau, H. Cramail and J. M. Asua, *ACS Appl. Polym. Mater.*, 2020, **2**, 4016–4025.
45 M. Manea, A. Chemtob, M. Paulis, J. C. de la Cal, M. J. Barandiaran and J. M. Asua, *AIChE J.*, 2007, **54**, 289–297.
46 Y. Ou, Z. Zhang, Z. Tang, Z. Yang, Y. Zhang, L. Tao, T. Wang, Q. Wang and S. Chen, *J. Polym. Sci.*, 2023, **61**, 1360–1371.
47 Z. Feng, W. Zhao, Z. Liang, Y. Lv, F. Xiang, D. Sun, C. Xiong, C. Duan, L. Dai and Y. Ni, *ACS Appl. Mater. Interfaces*, 2020, **12**, 11005–11015.
48 M. Mahapatra, M. Bourguignon, B. Grignard, M. Vandevenne, M. Galleni and C. Detrembleur, *Angew. Chem., Int. Ed.*, 2025, **64**, e202413605.
49 X. Chen, X. Liu, J. Lei, L. Xu, Z. Zhao, F. Kausar, X. Xie, X. Zhu, Y. Zhang and W. Z. Yuan, *Mol. Syst. Des. Eng.*, 2018, **3**, 364–375.
50 P. Liao, J. Huang, Y. Yan and B. Z. Tang, *Mater. Chem. Front.*, 2021, **5**, 6693–6717.

51 J. L. J. van Velthoven, L. Gootjes, D. S. van Es, B. A. J. Noordover and J. Meuldijk, *Eur. Polym. J.*, 2015, **70**, 125–135.
52 A. S. Pakdel, E. Niinivaara, E. D. Cranston, R. M. Berry and M. A. Dubé, *Macromol. Rapid Commun.*, 2021, **42**, 2000448.
53 J. Bergfreund, Q. Y. Sun, P. Fischer and P. Bertsch, *Nanoscale Adv.*, 2019, **1**, 4308–4312.
54 M. Bourguignon, J.-M. Thomassin, B. Grignard, C. Jerome and C. Detrembleur, *ACS Sustainable Chem. Eng.*, 2019, **7**, 12601–12610.